Applied Catalysis B: Environmental 126 (2012) 239–248

Contents lists available at SciVerse ScienceDirect

Applied Catalysis B: Environmental

journal homepage: www.elsevier.com/locate/apcatb

TAP investigation on methane conversion on supported Pd and Rh based catalysts – 1. Kinetics of methane adsorption

Y. Renème[a], F. Dhainaut[b], S. Pietrzyk[b,1], M. Chaar[c], A.C. van Veen[c], P. Granger[a,*]

[a] Unité de Catalyse et de Chimie du Solide, UMR CNRS 8181, Université de Lille 1, Sciences et Technologies, Cité scientifique, bâtiment C3, 59650 – Villeneuve d'Ascq Cedex, France
[b] Ecole Nationale Supérieure de Chimie de Lille, bâtiment C7, Cité scientifique, 59652 – Villeneuve d'Ascq, France
[c] Ruhr-University Bochum, Laboratory of Industrial Chemistry, Universitätsstraße 150, D44780 Bochum, Germany

ARTICLE INFO

Article history:
Received 27 March 2012
Received in revised form 6 June 2012
Accepted 12 June 2012
Available online 20 July 2012

Keywords:
TAP reactor
Methane activation
Palladium
Metal/support interface
NGV catalyst
Thermal aging

ABSTRACT

The adsorption of methane on supported Pd- and Rh-based catalysts has been investigated by TAP experiments in the temperature range of 400–550 °C. Particular attention was paid to the effects related to thermal aging causing significant particle growth which strongly alters the adsorptive properties of noble metals. In the temperature range 400–550 °C, most of CH_4 is irreversibly adsorbed and converted into CO, H_2, CO_2 and H_2O at selectivities depending on the pre-reductive or oxidative thermal treatment prior to TAP measurements. Responses of single pulse experiments were modeled in order to determine the rate constant values for methane adsorption and the related activation barriers. The employed model uses diffusivities for gas phase species determined separately in the different zones of the micro-reactor assuming a Knudsen diffusion. A significant increase in the activation energy values on aged catalysts is noted suggesting drastic changes in the nature of the reaction pathways for the dissociation of methane and/or in the extent of interaction between noble metals and the support. Such observations are discussed in view of a possible involvement of spill-over effects from alumina support onto noble metal particles partly suppressed after aging because of significant alterations of the metal/support interface.

1. Introduction

Methane activation over noble metals has been the subject of a wide number of publications and review articles [1–4]. Palladium is well-recognized among the most active noble metals. Moreover, its peculiar properties to activate methane under lean or rich conditions still present a fascinating task especially for optimizing the catalytic properties of natural gas fuelled vehicles (NGV) catalysts. The nature and product distribution drastically depend on thermal pre-treatment and related surface changes. By way of illustration, oxidized surfaces are more active toward methane oxidation, whereas reduced ones predominantly catalyze reforming reactions. Under reactive conditions, at atmospheric pressure, the presence of hot spots due to an exothermic methane conversion might be considered as a serious obstacle to identify reliably the reaction mechanism [5]. Hence, the implementation of transient kinetic experiments involving pulse techniques helps to better understand chemical processes taking place over surface planes [6–9]. From those investigations, it was found that methane dissociation can be considered as a key step for further formation of CO and CO_2 via common intermediates [8]. However, surface chemistry is usually complex, especially the prediction and the elucidation of surface reconstructions that can take place in the course of the reaction further altering the nature and the rate of surface reactions [3].

In this context, the implementation of TAP experiments performed under ultra-high-vacuum (UHV) which concern a small fraction of active sites on clean surfaces can be useful to get accurate and quantitative information related to the nature of elementary steps involved in the conversion of methane, the nature of the rate controlling steps and the occurrence of spill-over effects that may influence the catalytic behavior. The rate of OH spill-over from alumina support onto Ru particles was found kinetically significant in the partial oxidation of methane and has been already envisaged to emphasize the real importance of the metal/support interface [10]. Despite the pressure gap, interesting correlations were reported which demonstrated that optimized kinetic parameters from TAP measurements can correctly model steady state kinetic experiments at higher pressure conditions. This shows that the TAP approach can be considered as a powerful advanced kinetic strategy at the boundary between conventional kinetics and surface sciences [11].

This paper deals with the methane activation on Pd and Rh based catalysts based on single pulse TAP experiments. The associated modeling using the 1-D approximation, assuming a Knudsen

* Corresponding author. Tel.: +33 320 434 938; fax: +33 320 436 561.
E-mail addresses: stanislas.pietrzyk@ec-lille.fr (S. Pietrzyk), Pascal.granger@univ-lille1.fr (P. Granger).
[1] Tel.: +33 0951161541; fax: +33 320 436 561.

0926-3373/$ – see front matter © 2012 Elsevier B.V. All rights reserved.
http://dx.doi.org/10.1016/j.apcatb.2012.06.033

Table 1
Textural and surface properties of freshly-prepared and aged supported Pd and Rh based catalysts.

Catalyst		Specific surf. area ($m^2\ g^{-1}$)	D^a	d^b (nm)	Amount of accessible sites[c]	B.E. (eV)[d]		Surface composition[d]	
						Pd $3d_{5/2}$	Rh $3d_{5/2}$	Pd/Al	Rh/Al
Pd/Al_2O_3	Fresh	149	0.26	4.3	3.67×10^{22}	336.9	–	5.6×10^{-3}	–
	Aged	95	0.13	8.8	1.87×10^{22}	337.3	–	3.1×10^{-3}	–
$Pd–Rh/Al_2O_3$	Fresh	144	0.31	3.5	4.70×10^{22}	336.8	309.0	8.9×10^{-3}	1.0×10^{-3}
	Aged	91	0.21	5.4	3.19×10^{22}	337.3	310.5	2.2×10^{-3}	1.0×10^{-3}

[a] Metal dispersion from H_2 titration at 100 °C.
[b] Calculated from the metal dispersion assuming hemispherical particles.
[c] Expressed per kg_{cata}.
[d] From XPS analysis.

diffusion regime was used to get kinetic parameters representative of surface changes on NGV catalysts described elsewhere [12]. Particular attention was paid toward the impact of surface reconstructions on the nature and the rates of steps involved during methane dissociation after thermal aging, in simulated conditions that mimic those occurring under typical running conditions.

2. Experimental

2.1. Catalyst preparation and characterization

Supported Pd and Rh-based catalysts supplied by Umicore A.G. were prepared via a conventional wet impregnation of γ-Al_2O_3 support (Sasol 250 $m^2\ g^{-1}$) with aqueous rhodium and palladium nitrate solutions with concentrations adjusted to obtain 2.5 and 0.18 wt.% palladium and rhodium, respectively. Precursors thus obtained were successively calcined in air at 500 °C and then reduced in pure H_2 at 500 °C. Thermal aging was performed at 980 °C in wet atmosphere with 10 vol.% H_2O diluted in air. Specific surface areas were determined by nitrogen physisorption at −196 °C. Pore size analysis based on N_2 physisorption and mercury porosimetry reported in Fig. 1 reveals the presence of a bimodal distribution for freshly-prepared catalysts. Characterization of the surface properties of the catalysts is reported in Table 1. Metal dispersion was calculated from H_2 chemisorption performed at 100 °C using a pulse technique on catalyst pre-reduced in pure H_2 at 500 °C and assuming an atomic H/M ratio ~1 (M = Pd or Rh). X-ray photoelectron spectroscopic (XPS) measurements were carried out on calcined catalysts in a vacuum generators Escalab 220XL spectrometer, under ultra-high-vacuum (~10^{-10} Torr), equipped with a monochromatic aluminum source for excitation. Binding energy (B.E.) values were referenced to the binding energy of the Al 2p core level (74.6 eV in Al_2O_3). Data collected in Table 1 revealed the detrimental effect of thermal aging both on the specific surface area and on the metal dispersion probably due to thermal sintering phenomena activated at high temperature and wet atmosphere. XPS also revealed significant changes in the local environment of Pd^{2+} and Rh^{3+} species after thermal aging especially on the bimetallic catalysts accompanied with a significant surface Rh enrichment as earlier discussed [12].

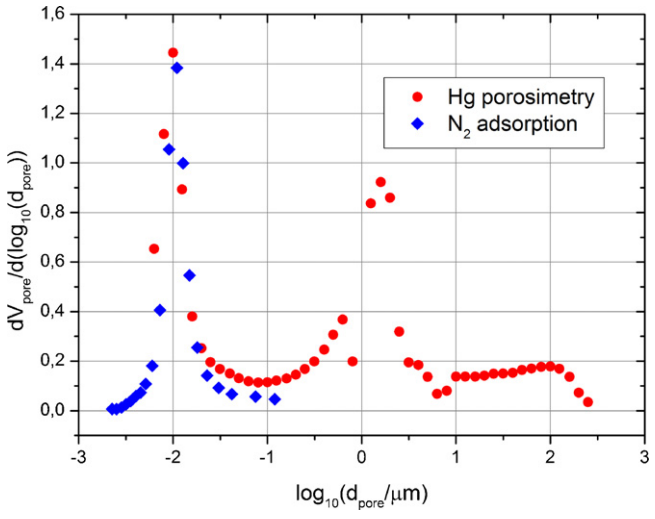

Fig. 1. Pore size distribution of freshly-prepared $Pd–Rh/Al_2O_3$, from mercury porosimetry (Hg) and nitrogen physisorption measurements at −196 °C.

2.2. TAP measurements

2.2.1. Experimental device

The TAP-1 instrument made use of two individual high speed pulse valves and enabled in situ pretreatments up to atmospheric pressure imminently to pulse experiments employing the so-called high pressure assembly [13]. Its micro-reactor made of stainless steel with quartz insert was previously described in detail [14]. The temperature profile inside reactor $T(x)$ was measured for different controlled oven temperatures T_0 (see Fig. 2). It was found that the mean values for all oven temperatures in the interval 300–600 °C can be adequately represented by a 3rd order polynomial in x. This polynomial was used in the reactor modeling to represent the temperature field. Inner diameter of the silica insert was 4 mm. In a typical experiment, the micro-reactor comprised 6 sections including a free volume in the inlet tube (length 8 mm, inner diameter 0.9 mm), a 4 mm layer of quartz wool (QW1), a 4 mm layer of inert silica (I1), a 3 mm layer of catalyst (C), an 8 mm layer of inert (I2), and a 4 mm layer of quartz wool (QW2) (see Fig. 2).

2.3. TAP experiments

In all '*single pulse*' experiments (SP), the QMS was tuned to m/z = 40 (Ar), 20 (Ne, Ar^{2+}), 15 (CH_4), 32 (O_2), 44 (CO_2), 28 (CO, CO_2, N_2), 2 (H_2, CH_4) and 18 (H_2O). The calibration with respect to the main components was performed in separate experiments with CH_4–Ar, CO–Ar and O_2–Ne mixtures, with the micro-reactor filled with quartz wool and silica inert only. The contribution of CH_4 to m/z = 2 and that of CO_2 to m/z = 28 were estimated by careful examination of SP data.

The micro-reactor charged as specified above was placed in the TAP reactor and heated in vacuum till 550 °C with the temperature rise of 40 °C min^{-1}, held at that temperature for 5 min and cooled down to 450 °C. At this temperature, the catalyst was reduced under a continuous flow of 72 mbar H_2 for 30 min. The reduction was followed by SP experiments with CH_4–Ar mixture, repeated 20 times successively for all 8 indicated m/z values. Each separate cycle corresponding to a specific m/z value consisted of 0.1 s of base-line level collection, of the first pulse, unique in SP experiments, at

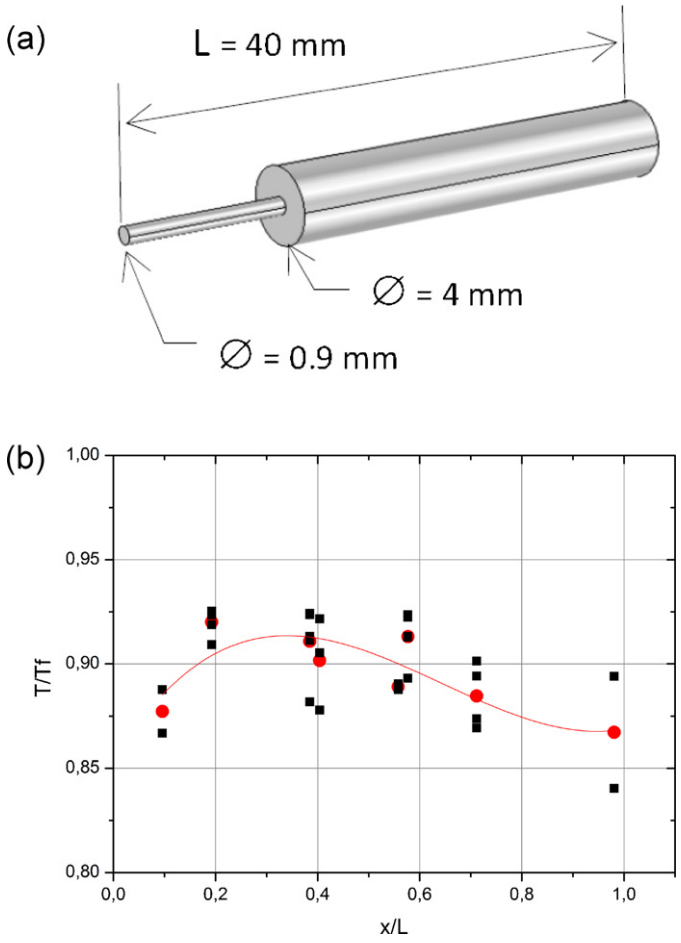

Fig. 2. TAP micro-reactor design (a) and temperature changes along the *x* axis (b).

0.1 s, followed 0.5 s later in alternative pulse (AP) experiments by another one. The total time was equal to 4 s. The same sequence of SP and AP experiments was repeated at 450 °C, 500 °C, 550 °C and finally 400 °C. The temperature changes occurred under H_2 flow for ensuring the reduced state of the catalyst. The obtained results were referred to as those for '*reduced catalysts*'. For '*oxidized catalysts*', results were obtained after heating the micro-reactor under flowing O_2 at 450 °C for 50 min. The same series of experiments as above-mentioned was performed at similar temperatures. During the changes of temperature the catalyst was exposed to oxygen flow.

3. Results and discussion

An example of averaged rough data for aged, reduced Pd–Rh catalyst at 450 °C is illustrated in Fig. 3. Since the baseline levels for some *m*/*z* values were time dependent, these levels were subtracted individually for each pulse before averaging. The corrections for fragmentation were also introduced individually for each pulse. Corrected data are reported in Fig. 3b and c for pre-reduced and pre-oxidized samples, respectively. As shown, the nature of the thermal pre-treatment significantly alters the nature of the products with CO and H_2 predominantly formed on a reduced surface whereas a pre-oxidized surface essentially leads to CO_2 production. Returning to pre-reduced samples, the shape of the outlet flow rate of hydrogen suggests the existence of two parallel pathways. A fast process initially takes place which is not correlated to CO production and can be likely ascribed to methane decomposition. Afterwards, a slower H_2 production is discernible which coincides with CO production. Large negative signal for CO_2 is also noticeable and signifies that its high and variable baseline level results from slow reaction/desorption of accumulated surface species. On the same catalyst in its oxidized state, at 550 °C (Fig. 3c) the sole production of CO_2 emphasizes a fast oxidation of CO and H_2. There is a negative signal for H_2O. This behavior is typical of all experiments on Pd and Pd–Rh catalysts indicating a slow release of H_2O from the catalyst, which is perturbed upon pulse introduction. The perturbation of H_2O release is caused by the consumption of adsorbed water in a reaction with methane. Similar experiments repeated on aged samples did not reveal significant changes except the shape of the H_2 exit curve illustrated on pre-reduced Pd–Rh/Al_2O_3 in Fig. 4. As observed, while the fast H_2 production predominates, the slow process previous depicted on fresh catalyst seems to be attenuated after aging.

3.1. Qualitative analysis of methane outlet flow curves

The description of mass transport and reaction processes in TAP reactor requires a mathematical model that accounts for these phenomena for further estimation of the kinetic parameters. For the pulse sizes investigated in our TAP experiments, the Knudsen diffusion regime likely prevails which should insure the absence of significant external mass and heat transfer limitations and facilitate the modeling of mass transport phenomena. On the contrary, the presence of rather narrow mesopores (about 10 nm, Fig. 1) may represent a source of perturbations [15].

Outlet methane flow curves have been normalized with respect to the initial pulse methane contents and compared with the corresponding normalized argon curves. Such a comparison for a 1-zone TAP reactor is meaningful if performed in reduced variables, $F_i/(D_i/(\varepsilon L^2))$ vs. $tD_i/(\varepsilon L^2)$, where F_i stands for the normalized pulse intensity of the gas species *i*, D_i the effective Knudsen diffusivity at the temperature inside the catalyst bed, ε the catalyst bed porosity and *L* the bed length [16]. Such a treatment minimizes the influence of different D_i values for different species. Indeed, in a more realistic case of a multi-zone bed, each zone is characterized by its particular porosity and length, and the Knudsen diffusivity coefficient for each species $D_{i,z}$ is given by Eq. (1):

$$D_{i,z} = D_z^0 \sqrt{\frac{T_z}{M_i}} \quad (1)$$

where T_z is zone temperature and M_i molar weight of the diffusing species *i*. Since for each zone all parameters T_z, ε, L_z and D_z^0 may be assumed constant, the comparison of the species with different molar masses may be achieved using variables $F_i{M_i}^{1/2}$ vs. $t/{M_i}^{1/2}$ [17]. Taking the difference of molar weight between two gases into account, their corresponding outlet flow rates have been converted in variables $F_i{M_i}^{1/2}$ vs. $t/{M_i}^{1/2}$, where F_i (pulse intensity) stands for the normalized flow rate according to the methodology earlier described [16] for a 6 zone micro-reactor (free space included). The results presented in Figs. 5–8 refer to SP experiments performed at 450 °C on Pd/Al_2O_3 and Pd–Rh/Al_2O_3. Corresponding experimental data recorded 400, 500 and 550 °C are reported in Figs. S1–S3 which illustrate similar trends for all the temperatures. As seen in Figs. 5–8, methane adsorption is irreversible in all cases, irrespective of the reductive/oxidative pre-treatment and the selected temperature, since the methane curves are located below those corresponding to the inert gas, without crossing. In addition, data reported in Table 2 indicates that most of the methane adsorbed on Pd/Al_2O_3 and Pd–Rh/Al_3O_3 is subsequently converted. Such observations emphasize a direct dissociative process rather than a precursor-mediated mechanism involving a molecular precursor state as proposed elsewhere [18,19]. Another remarkable result reported in Fig. 5b for aged Pd-only catalyst, preliminary

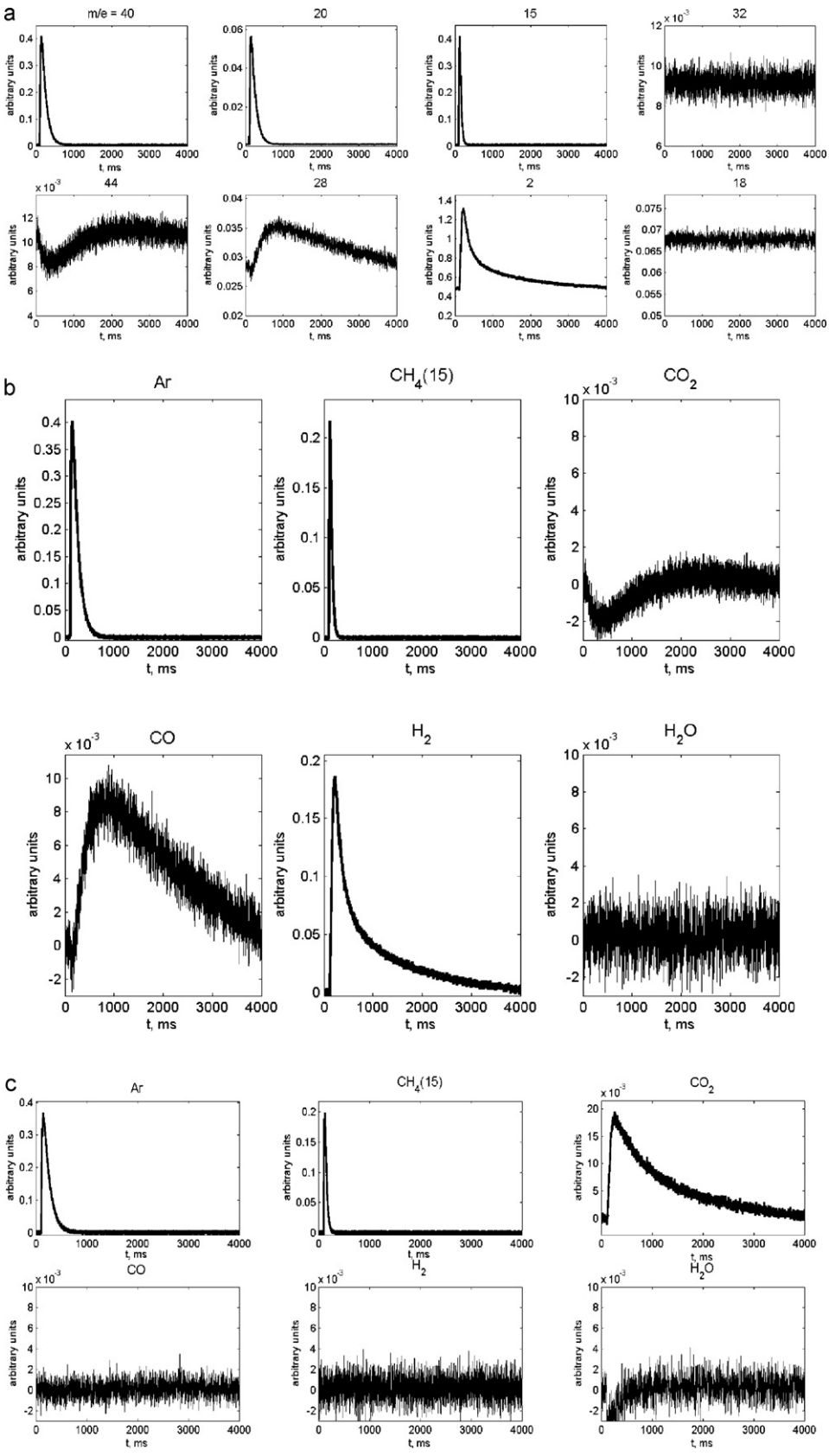

Fig. 3. MS responses during TAP experiments on aged Pd–Rh/Al_2O_3 performed at 550 °C: rough data on pre-reduced sample (a), corrected data on pre-reduced (b) and oxidized sample (c).

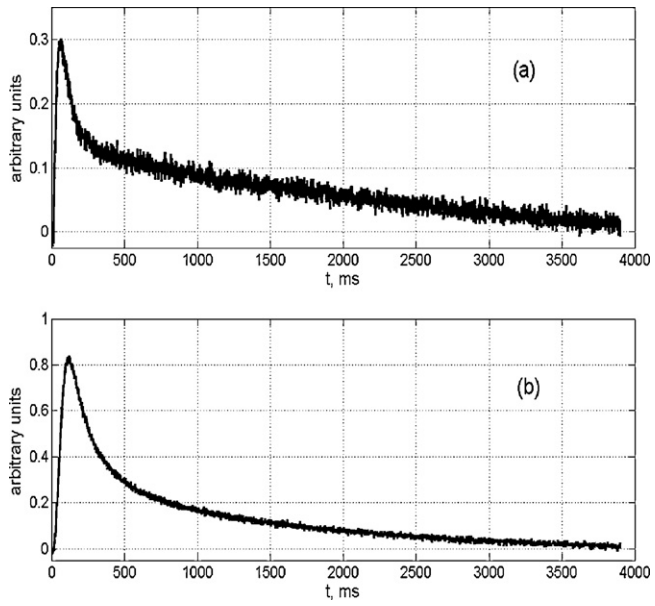

Fig. 4. Hydrogen outlet flow rate from TAP experiments on pre-reduced Pd–Rh/Al_2O_3 performed at 550 °C: fresh sample (a), and aged sample (b).

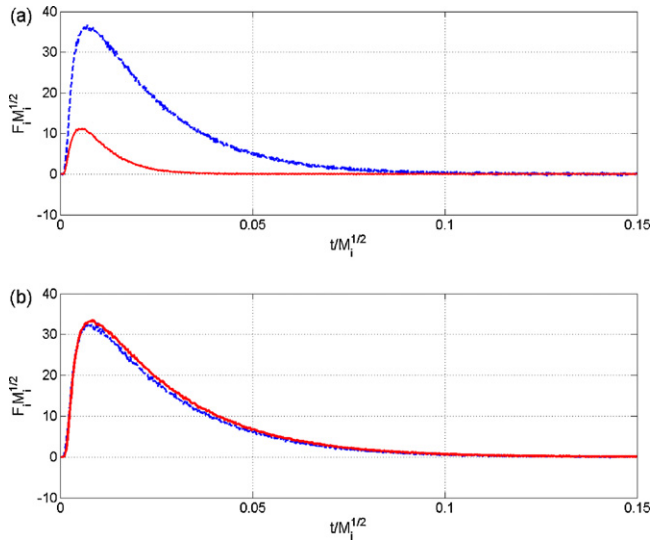

Fig. 5. Comparison of normalized CH_4 and Ar outlet flow curves $F_iM_i^{1/2}$ vs. $t/M_i^{1/2}$ recorded on pre-reduced Pd/Al_2O_3 at 450 °C where F_i stands for the pulse intensity-normalized flow multiplied by $M_i^{1/2}$ with M_i representing molar weight of the component i – freshly-prepared sample (a); aged sample (b).

Table 2
Fraction of methane converted during a single pulse TAP experiment at different temperatures.

Catalysts	Pretreatment	Temperature SP experiment (°C)			
		400	450	500	550
Pd/Al_2O_3	Reduced	0.84	0.86	0.88	0.87
	Oxidized	0.88	0.88	0.88	0.89
Aged-Pd/Al_2O_3	Reduced	0.01	–	0.08	0.21
	Oxidized	0.58	0.69	0.81	0.84
Pd–Rh/Al_2O_3	Reduced	0.85	0.86	0.88	0.88
	Oxidized	0.84	0.86	0.85	0.85
Aged-Pd–Rh/Al_2O_3	Reduced	0.55	0.72	0.79	0.81
	Oxidized	0.57	0.70	0.77	0.82

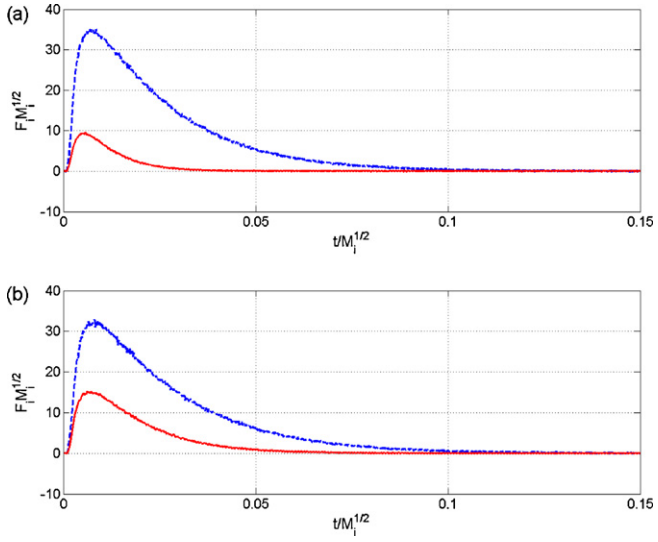

Fig. 6. Comparison of normalized CH_4 and Ar outlet flow curves $F_iM_i^{1/2}$ vs. $t/M_i^{1/2}$ recorded on pre-oxidized Pd/Al_2O_3 at 450 °C where F_i stands for the pulse intensity-normalized flow multiplied by $M_i^{1/2}$ with M_i representing molar weight of the component i – freshly-prepared sample (a); aged sample (b).

reduced, is related to the superimposition of the experimental and reference curves associated to methane and Ar respectively, indicating very low methane adsorption at 450 °C and at 400 °C (see Supplementary material, Fig. S1(c)). On the contrary, thermal aging of Pd–Rh catalyst does not exert such a dramatic influence, although methane adsorption is still much lower than that on fresh catalyst (Figs. 7 and 8). Hence, rhodium incorporation to Pd would preserve the Pd capacity toward methane adsorption and related conversion. As exemplified in Table 2, this conversion is rather similar between the corresponding oxidized and reduced catalysts with a notable exception of aged Pd-only catalyst. In all cases, methane adsorption on aged catalysts is weakened compared with the fresh ones. This can be likely related to a lower Pd dispersion due to thermal sintering in agreement with hydrogen chemisorption data reported in Table 1, possibly combined with other surface

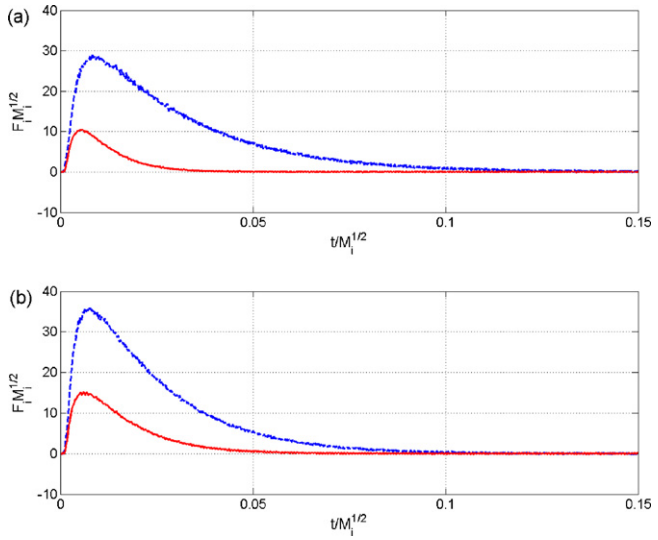

Fig. 7. Comparison of normalized CH_4 and Ar outlet flow curves $F_iM_i^{1/2}$ vs. $t/M_i^{1/2}$ recorded on pre-reduced Pd–Rh/Al_2O_3 at 450 °C where F_i stands for the pulse intensity-normalized flow multiplied by $M_i^{1/2}$ with M_i representing molar weight of the component i – freshly-prepared sample (a); aged sample (b).

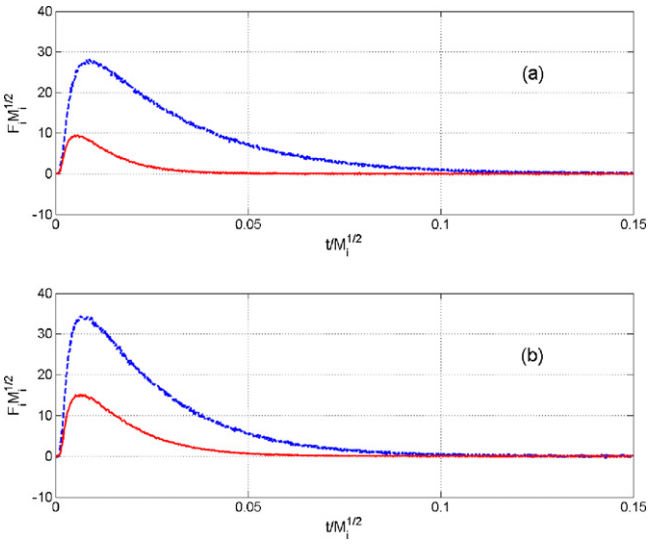

Fig. 8. Comparison of normalized CH_4 and Ar outlet flow curves $F_iM_i^{1/2}$ vs. $t/M_i^{1/2}$ recorded on pre-oxidized Pd–Rh/Al_2O_3 at 450 °C where F_i stands for the pulse intensity-normalized flow multiplied by $M_i^{1/2}$ with M_i representing molar weight of the component i – freshly-prepared sample (a); aged sample (b).

modifications, especially in the case of bimetallic catalysts with relative changes of the surface Rh/Pd ratio after aging (see Table 1).

3.2. Estimation of rates and activation energies for methane adsorption on fresh and aged supported Pd and Rh based catalysts

Modeling of TAP experiments was performed using COMSOL Multiphysics, version 3.5a to build models, and Matlab R2009b to compare experimental data with modeling results, using COMSOL models converted to Matlab m-files as a basis of Matlab objective functions. The model parameters were optimized using Matlab '*fminsearch*' function, based on the Nelder–Mead algorithm.

3.2.1. Modeling of methane adsorption

The flexibility of COMSOL allows easy building of different models, and Matlab is particularly adapted to exploit huge sets of data as these produced from TAP experiments. The modeling was performed using 1D approximation according to the partial differential equation (2) which accounts for transient Knudsen diffusion for gas-phase species i.

$$\frac{\partial c_i}{\partial t} = \frac{\partial}{\partial x}\left(\frac{D_{i,z}}{\varepsilon_z}\frac{\partial c_i}{\partial x}\right) + R_i \tag{2}$$

with,

$$D_{i,z} = D_z^0\sqrt{\frac{T(x)}{M_i}} \tag{3}$$

where $D_{i,z}$ is effective Knudsen diffusivity of gas species i in the zone z, M_i is molar mass of the species i in g mol^{-1}, R_i is the local rate for the production of i in mol m$_{bed}^{-3}$ s^{-1} and $T(x)$ the local temperature. Inlet border condition was taken as '*flux*', expressed by Eq. (4).

$$F_i(t) = \frac{N_i^0}{A_r N_A}\frac{t}{\tau^2}\exp(-t/\tau) \tag{4}$$

where N_i^0 is the number of molecules of i in a single pulse, A_r is reactor area, N_A is the Avogadro's number and τ a constant determining the pulse width [17,20,21]. Outlet boundaries conditions were taken as '*Concentration*' for each gas phase species i, with $c_i = 0$. For inner boundaries the default condition '*Continuity*' (that of the fluxes) was retained. For surface species, the partial differential equation (5) has been taken into account,

$$\frac{\partial \theta_i}{\partial t} = r_i \tag{5}$$

θ_i represents the surface coverage of the species i, and r_i stands for the turnover number in s^{-1}. However, in the modeling presented in this study, limited to the methane adsorption, the surface species were not taken into account. The surface coverage of free sites was considered as 1, since the pulse size to the amount of hydrogen adsorption site ratio in the catalyst bed was always less than 0.2%.

To determine the parameters of these equations (D_z^0, rate constants in R_i), Comsol models were converted to Matlab m-files, and developed into Matlab functions computing objective functions equal to the sum of the square differences between experimental and computed CH_4 outlet flow rate values. In real TAP experiments, the solids in the micro-reactor (catalyst or inert powder) are maintained by means of metal grids or quartz wool. Their contribution to the observed phenomena is usually included into those of the adjoining solid layer. Here, an attempt was achieved to model these additional components explicitly, as separate solid zones. As already indicated, the micro-reactor used in this study contains 6 zones. The inlet zone has been neglected because of its small volume, equivalent to 0.4 mm of the main section of the reactor. The remaining 5 zones include 2 silica wool zones, 2 silica powder (inert) zones and the catalyst zone. The diffusivity parameters D^0 for the three solids involved have been determined successively.

First, some SP experiments with a 1:1 Ar–Ne mixture have been performed with the micro-reactor containing quartz wool and considering two different loadings. Initially, the 4 mm diameter reactor was loaded with a 28 mm layer of quartz wool. Secondly, 20 mm layer of quartz wool was preceded by 10 mm of free space. Oven temperatures varied in the range 200–360 °C, and the pulse sizes varied between 2×10^{14} and 1×10^{15} gaseous molecules for the first loading, and between 1.4×10^{14} and 1.4×10^{15} gaseous molecules for the second one. Diffusivities in the free volume, present in the second case, were calculated using the classical Eq. (6).

$$D_i = \frac{2d}{3}\sqrt{\frac{2000RT}{\pi M_i}} \tag{6}$$

The parameter d stands for the reactor diameter and $R = 8.3144$ J mol^{-1} K^{-1} the ideal gas constant. The mean values of (D^0/ε) obtained by optimization were practically identical for Ar and Ne data but different for the two loadings: 3.94×10^{-3} and 4.04×10^{-4} m^2 s^{-1} for Ar and Ne, respectively, for the first case, and 3.36×10^{-4} m^2 s^{-1} for both gases in the second case. Such relatively important differences can be attributed to a poor reproducibility of the quartz wool properties, depending on its compacting. For further modeling, the mean value of 3.6×10^{-3} m^2 s^{-1} was used for quartz wool layers. Both, their mass and length were kept constant at 10 mg and 4 mm, respectively.

The apparent density of the quartz wool layers in the reactor was about 200 kg m^{-3} which corresponds to a void fraction (porosity) of 0.91. Recent literature data [22] provide for quartz wool layers, exhibiting the same porosity, an estimation of the tortuosity τ' of about 1.1. Hence, according to Eq. (7), the above-mentioned D^0/ε values would correspond to d_{pore} of 82 μm, which seems plausible for a quartz wool with fibers thickness of 100 μm.

$$\frac{D^0}{\varepsilon} = \frac{2d_{pore}}{3\tau'}\sqrt{\frac{2000R}{\pi}} \approx \frac{48.5d_{pore}}{\tau'} \tag{7}$$

$(D^0/\varepsilon)_i$, for the nonporous silica powder was determined from the outlet flow rate curves obtained during the calibration performed with the mixtures CH_4–Ar and O_2–Ne. The micro-reactor

was loaded with 3 layers of solids: 4 mm of quartz wool, 18 mm of silica powder and 4 mm of quartz wool. The modeling of this micro-reactor, taking D^0/ε previously estimated for the quartz wool of 3.6×10^{-3} m^2 s^{-1} into account, provides a mean of 9 values of $(D^0/\varepsilon)_i$ equal to 6.935×10^{-4} m^2 s^{-1}, with a standard deviation on the average value equal to 0.066×10^{-4} m^2 s^{-1}. For further modeling, a value of 6.94×10^{-4} has been considered.

Taking for the tortuosity a typical value for nonporous beds equal to 1.5 into account [23], one obtains for d_{pore} a value of 22 μm. This value is lower than that expected from the correlation of Huizenga–Smith [23] given from Eq. (8),

$$d_{pore} = \frac{2}{3} d_{particle} \frac{\varepsilon_b}{1 - \varepsilon_b} \quad (8)$$

where ε_b stands for the bed porosity which gives for a bed of inert, with particle size between 160 and 250 μm and a typical porosity of 0.4, a numerical values for d_{pore} in the range of 71–112 μm. However, inert porosities, as low as 0.25, were reported in the literature [21,24]. For a porosity of 0.3 this range becomes narrower of approximately 32–50 μm, and a slightly higher tortuosity of 2 provides for d_{pore} a value of 29 μm. Therefore, the estimated value of D^0/ε for the inert may be considered as acceptable.

In both previous models the term accounting for chemical reaction R_i was assumed nil. To model the experiments in SP format with CH_4–Ar mixture, this term is 0 for Ar, but not for CH_4. Accordingly to the results of the preliminary analysis presented before, the adsorption of CH_4 was considered as irreversible. Therefore, Eq. (9) can be established

$$R_{CH_4} = -k_a \rho_b c_{CH_4} \quad (9)$$

with a bed density $\rho_b = 530\,kg\,m^{-3}{}_{bed}$ and adsorption rate constant k_a in $m^3_{gas}/(kg\,s)$. Outlet flow rate curves of CH_4 and Ar were modeled as explained previously, with the values of (D^0/ε) of the catalyst, whereas $(D^0/\varepsilon)_c$, and k_a/ε were considered as adjustable parameters. Equation (9) implies approximately constant θ_v corresponding to the fraction of vacant sites, that is a usual assumption for TAP experiments. This hypothesis seems adequate since the order of magnitude of the pulse size (CH_4) to the amount of active site ratios calculated from hydrogen was always lower than 2×10^{-3}. However, in some cases an evolution of the exit CH_4 curves with pulse number was observed, particularly for oxidized catalysts, which could be attributed to a relatively important number of amu measured (8 amu), large number of ad-species remaining at the surface after adsorption and surface reaction of one methane molecule, and some possible loss of active sites following the treatment of a catalyst. To limit the influence of these variations, only the averages of the first 6 pulses out of 20 were used in the modeling. Objective function was the sum of the square differences between experimental and calculated outlet flows for both gases.

Estimated values of the diffusivity constants $(D^0/\varepsilon)_c$ in Table 3 are rather low, approximately 10 times lower than that for the inert silica, in spite of rather similar granulometry for both solids. This may result from a developed porous structure of the catalyst contrasting with its absence in the case of silica powder. The relative importance of the porous structure depends on the ratio of characteristic times for the inter-granular space in the bed and that for the catalyst's grains, expressed e.g. by a factor γ [15]:

$$\gamma = \frac{L^2 \varepsilon_b / D_b}{R_p^2 \varepsilon_p / D_p} \quad (10)$$

L is the bed length, R_p the mean particle radius, and the indices 'b' and 'p' mean "bed" and "pores of the particle" respectively. For a

Table 3
Sensitivity of the estimated value for $(D^0/\varepsilon)c$ on Pd/Al_2O_3 and $Pd–Rh/Al_2O_3$ according to the reductive or oxidative thermal treatment and the aging process under simulated condition at 980 °C in wet atmosphere (10 vol.% H_2O in air).

Catalyst	Activation thermal treatment	Temperature (°C)				Average $(D^0/\varepsilon)c$	Standard deviation	Average $(D^0/\varepsilon)c$
		400	450	500	550			
Pd/Al_2O_3	Oxidized[a]	5.30×10^{-5}	5.61×10^{-5}	5.82×10^{-5}	5.97×10^{-5}	5.68×10^{-5}	0.29×10^{-5}	5.86×10^{-5}
	Reduced[b]	5.70×10^{-5}	5.84×10^{-5}	6.18×10^{-5}	6.48×10^{-5}	6.05×10^{-5}	0.35×10^{-5}	
Aged-Pd/Al_2O_3	Oxidized[a]	5.12×10^{-5}	5.78×10^{-5}	6.22×10^{-5}	6.53×10^{-5}	5.91×10^{-5}	0.61×10^{-5}	5.90×10^{-5}
	Reduced[b]	5.69×10^{-5}	6.07×10^{-5}	5.97×10^{-5}	5.79×10^{-5}	5.88×10^{-5}	0.17×10^{-5}	
$Pd–Rh/Al_2O_3$	Oxidized[a]	5.14×10^{-5}	5.28×10^{-5}	5.59×10^{-5}	5.98×10^{-5}	5.50×10^{-5}	0.37×10^{-5}	5.53×10^{-5}
	Reduced[b]	5.10×10^{-5}	5.46×10^{-5}	5.64×10^{-5}	6.03×10^{-5}	5.56×10^{-5}	0.39×10^{-5}	
Aged-$Pd–Rh/Al_2O_3$	Oxidized[a]	5.89×10^{-5}	6.39×10^{-5}	7.02×10^{-5}	7.61×10^{-5}	6.73×10^{-5}	0.75×10^{-5}	6.75×10^{-5}
	Reduced[b]	6.08×10^{-5}	6.57×10^{-5}	6.99×10^{-5}	7.42×10^{-5}	6.77×10^{-5}	0.57×10^{-5}	

[a] After heating under flowing O_2 at 450 °C for 50 min.
[b] After heating under a continuous flow of 72 mbar H_2 at 450C for 30 min.

Table 4
Results of the optimization on Pd–Rh/Al_2O_3.

Catalyst	Thermal pretreatment	T_0 (°C)[a]	D_b^0 [b]	D_p^0 [c]	A_0 ($m^2\ m_{bed}^{-3}$)[d]	L_0 (μm)[e]	F_{min} [f]
Fresh-Pd–Rh/Al_2O_3	Reduced	400	1.16×10^{-4}	7.22×10^{-8}	3.50×10^{-4}	120	2.910
		450	1.36×10^{-4}	8.33×10^{-8}	3.97×10^{-4}	116	3.561
		500	1.38×10^{-4}	7.63×10^{-8}	4.18×10^{-4}	110	3.346
		550	1.48×10^{-4}	13.9×10^{-8} [g]	3.30×10^{-4}	140	4.240
	Oxidized	400	1.20×10^{-4}	14.25×10^{-8} [g]	2.68×10^{-4}	164	2.132
		450	1.26×10^{-4}	8.22×10^{-8}	3.70×10^{-4}	122	3.249
		500	1.28×10^{-4}	8.46×10^{-8}	3.64×10^{-4}	118	3.911
		550	1.36×10^{-4}	9.21×10^{-8}	3.58×10^{-4}	118	3.669
Aged-Pd–Rh/Al_2O_3	Reduced	400	1.52×10^{-4}	10.87×10^{-8}	2.62×10^{-4}	126	3.403
		450	1.51×10^{-4}	10.49×10^{-8}	2.54×10^{-4}	113	4.654
		500	1.52×10^{-4}	9.94×10^{-8}	2.61×10^{-4}	106	6.770
		550	1.69×10^{-4}	11.91×10^{-8}	2.67×10^{-4}	115	6.692
	Oxidized	400	1.54×10^{-4}	10.23×10^{-8}	2.73×10^{-4}	124	4.257
		450	1.58×10^{-4}	11.17×10^{-8}	2.68×10^{-4}	125	4.707
		500	1.63×10^{-4}	10.26×10^{-8}	2.91×10^{-4}	114	4.641
		550	1.69×10^{-4}	9.71×10^{-8}	3.06×10^{-4}	106	9.446

[a] T_o oven temperature.
[b] Inter-granular diffusivity coefficient expressed in $(m^2\ s^{-1})(mol\ K^{-1})^{1/2}$.
[c] Diffusivity coefficient for mesopores expressed in $(m^2\ s^{-1})(mol\ K^{-1})^{1/2}$.
[d] Surface of the grains per unit of volume of the bed ($m^2\ m_{bed}^{-3}$).
[e] Average length of mesopores.
[f] Value of the objective function at minimum; 1000 points in the interval (0.1 s), sum of square differences between area-normalized model and experimental Ar outlet flow rates.
[g] Neglected as outliers.

1-zone reactor, and a ratio of inter- and intra-particular tortuosities of 1/3, Eq. (10) is transformed into Eq. (11) [15]:

$$\gamma \cong 2\frac{1-\varepsilon_b}{\varepsilon_b}\frac{d_{pore}L^2}{d_{pellet}} \quad (11)$$

Taking, in the first approximation, $\varepsilon_b = 0.4$, $d_{pellet} = 200\ \mu m$, $L = 23$ mm, and d_{pore} equal to 1 μm (macropores) and 0.01 μm (mesopores, see Fig. 1) into account, then γ is equal to 200 for macropores and 2 for mesopores. The first value means that the characteristic time for the diffusion in the macropores is much smaller than that for the diffusion in inter-particle voids of the bed, and the concentration in the macropores should not differ significantly from those in the spaces between particles. On the contrary, these characteristic times are of the same order of magnitude for inter-particle spaces and for the mesopores, and the diffusion in these pores should influence the observed outlet flow rate curves.

Since the reduced and oxidized catalysts represent the same loading and differ only in the nature of the chemical treatment, large differences between the values of diffusivity parameters $(D^0/\varepsilon)_c$ obtained for each catalyst pre-activated differently are not expected. The ultimate mean values are indeed rather similar, so that the differences between individual values may be attributed to a rather small number of pulses taken into account for each temperature, limited to 6 pulses out of 20, according to previous explanations. Another interesting feature extracted from these data is a steady increase of D^0/ε with temperature, while this value should be constant for a given solid according to the theory of the Knudsen diffusion in catalytic beds composed of nonporous solids. This variation cannot be attributed to any slow evolution of the catalyst properties, because the sequence of temperature was always 450 °C, 500 °C, 550 °C and 400 °C (oven temperatures). This could be due to the differences between actual temperatures along the axis of the micro-reactor and the average function used to compute these temperatures, and to radial gradients of temperature in the catalytic bed which were not verified experimentally. Both effects should be correlated with the oven temperature. On the other hand, this behavior could result from an inadequacy of the applied model neglecting the presence of mesopores.

Therefore, an attempt was undertaken to take into account the influence of mesopores by a model similar to that earlier proposed by Phanawadee et al. [15]. The parameters of this last model are diffusivities (diffusivity constants) for the inter-particle space, those for the intra-particle void space representing the pores, and the mean particle radius used to estimate the surface of the particles per unit volume of the bed, and considered as equal to the pore length (pore tortuosity is included in the intra-particle diffusivity constant). However, according to the analysis of the above-mentioned characteristic times, the volume of the inter-particle space was augmented by that of the macropores, while the intra-particle void space was restricted to mesopores alone. Also, the surface contact between the two types of void spaces was considered as a separate parameter, independent of the particle radius. This model characterized by four parameters: D_b^0, D_p^0, A_0 and L_0, corresponding respectively to the diffusivity parameter for inter-granular diffusion (including macropores), diffusion in mesopores, surface contact mesopores/(macropores + interparticle voids) in $m^2\ m_{bed}^{-3}$, and average mesopore length, was applied to Ar effluent curves in all experiments on Pd–Rh/Al_2O_3 catalysts. The objective function was based on area-normalized exit flows. The porosities corresponding to both types of void spaces were estimated from porosimetry data determined on fresh Pd–Rh/Al_2O_3 catalyst. The results are given in Table 4. The first important conclusion is that the model reproduced very well the experimental curves, the average errors being of the order of 1% of the maxima of the area-normalized effluent curves, and due mostly to the noise in the experimental data. In addition, the values of the optimized parameters seem in relatively good agreement with the expected ones. The values of the first diffusivity parameter D_b^0, between 1.2×10^{-4} and 1.7×10^{-4}, are higher than those obtained previously, about 6×10^{-5} (see Table 3). These values are lower than those expected for inter-particle voids, about 1.5×10^{-3} (particle diameter 150 μm, porosity = 0.32, tortuosity = 1.5), but higher than the estimates for macropores, about 1×10^{-5} (pore diameter 1 μm, tortuosity = 5).D_p^0 value, characterizing mesopores, of about 8×10^{-8} for fresh Pd–Rh/Al_2O_3, substituted into Eq. (7), gives for the tortuosity a value of ~5, for a pore diameter of 8×10^{-9} m, corresponding to the maximum of the distribution curve (see Fig. 1).

Table 5
Estimates of kinetic parameters from the modeling of SP TAP experiments.

Catalyst		Pretreatment	k_{ads} [a]	Activation[b] energy (kJ mol^{-1})	R^2[c]
Pd/Al_2O_3	Fresh	Reduced	0.48	7.0	0.992
		Oxidized	0.55	5.0	0.967
	Aged	Reduced	0.01	45.0	0.339
		Oxidized	0.32	27.0	0.981
$Pd–Rh/Al_2O_3$	Fresh	Reduced	0.41	8.0	0.994
		Oxidized	0.43	6.0	0.974
	Aged	Reduced	0.29	28.0	0.947
		Oxidized	0.34	28.0	0.966

[a] m^3_{gas} kg^{-1} s^{-1}, at 700 K.
[b] Calculated from the slope of Arrhenius plots in Fig. 9.
[c] Regression coefficient.

This value agrees well with the data for alumina-supported catalysts quoted by Satterfield [25]. Estimated mean mesopore lengths obtained from this model are about 120 μm for all catalysts which seems in reasonable agreement with the granulometry of the catalyst.

The surface of contact between mesopores and remaining bed including interparticle voids and mesopores is about 4×10^4 m^{-1} for fresh $Pd–Rh/Al_2O_3$ catalyst. As expected, this value is higher than the external surface of a bed composed of spherical particles (2.7×10^4 m^{-1} for particle diameters of 150 μm and porosity of 0.32), but much lower than the surface area of macropores estimated from porosimetry measurements (about 2 m^2 g^{-1}, and 10^6 m^{-1} for a bed density of 530 kg m^{-3}). This unexpected result may be due to oversimplifications of the proposed model.

Finally, the diffusivity parameters for both types of voids increase on aging, suggesting an increase of the pore diameters, while the surface of contact decreases. Such tendency seems in reasonable agreement with expected changes in the porous structure between fresh and aged $Pd–Rh/Al_2O_3$. The estimated pore length does not change. Somewhat worse precision of adjustment for aged catalysts could be explained by some changes of the porosities due to aging, neglected in the modeling.

Therefore, the values of the diffusivity parameters obtained without taking into account explicitly the porous structure of the catalysts represent only synthetic global characteristics. For a catalyst with porosity characterized by the presence of narrow pores ~10 nm, the modeling of the diffusion should take into account their contribution. The details of the Comsol model are given as Supplementary material S4.

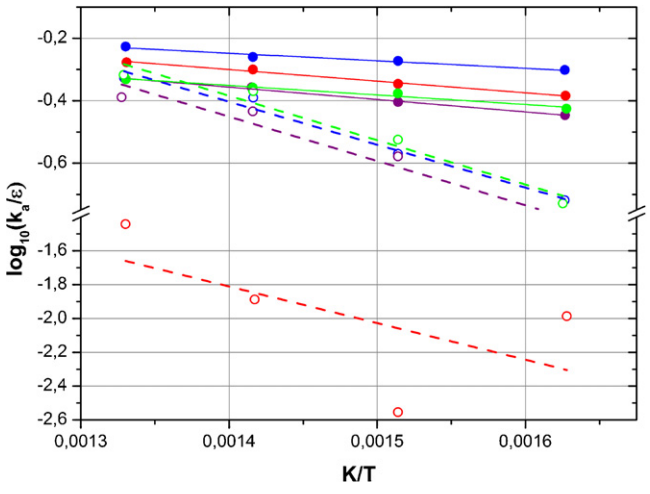

Fig. 9. Arrhenius plot for methane activation on fresh and aged Pd/Al_2O_3 and $Pd–Rh/Al_2O_3$-aged samples (dashed line); fresh samples (continuous line).

3.2.2. Comparison of the kinetic parameters and correlation with surface properties

Rate constants k_a at the temperatures selected for TAP measurements allow us to estimate the activation energy values for methane adsorption from the slope of the Arrhenius plots reported in Fig. 9. Results collected in Table 5, underline two different sets of values respectively calculated on freshly-prepared and aged catalysts in the range 5–8 kJ mol^{-1} and 28 kJ mol^{-1}, respectively. An abnormally high value, of approximately 45 kJ mol^{-1}, is likely overestimated on pre-reduced aged-Pd/Al_2O_3 with a poor accuracy reflected by the regression coefficient. In fact, such a wide deviation can be easily explained by considering the very low values for the rate constants extracted from the TAP responses on this catalyst. However, a significant deviation on the activation barrier on aged-Pd/Al_2O_3 cannot be completely ruled out as previously demonstrated [26,27] according to pre-reductive or oxidative thermal treatments and would reflect the existence of different reaction pathways for methane dissociation. The weak methane adsorption on pre-reduced fresh catalyst would suggest that only a limited number of active sites could be involved in methane activation [27]. A similar behavior was earlier evidenced on supported Rh and Ni based catalysts associated to a structure-sensitive reaction [26] as evidenced on single crystal surfaces. Dewaele et al. suggested the involvement of two different pathways for the activation of methane on Ni. As noted by those authors the loss of methane activation is caused by oxygen desorption and can be fully regenerated by an oxygen feed. This earlier observation strongly suggested that methane is activated on this type of sites through interaction with reversibly chemisorbed oxygen. However, those authors also evidenced that successive pulses induce a long-term deactivation process related to their progressive disappearance. A model description assumed the H abstraction from methane or related adsorbed intermediates via chemisorbed oxygen. In a first approach, such a proposal seems in rather good agreement with our observations since a pre-oxidation of aged-Pd/Al_2O_3 partly restores the adsorptive properties of palladium toward methane. However, such a feature is not reproduced on fresh samples particularly on $Pt–Rh/Al_2O_3$. Obviously, one has to mention that thermal aging has a detrimental effect. Interestingly, Rh incorporation to Pd seems to attenuate the impact of thermal aging notably after a pre-reductive thermal treatment since CH_4 adsorption is still preserved contrarily to previous observations on aged-Pd/Al_2O_3. In that case, the adsorption properties seems to be less sensitive to the nature of the thermal pre-treatment prior to methane adsorption with comparable rate constant and activation energy values of 28 kJ mol^{-1}. All these kinetic features must be related to surface reconstructions with a limited impact of thermal sintering when rhodium is incorporated to palladium.

Theoretical calculations earlier developed by Shustorovich and Sellers [28] based on the unity bond index-quadratic potential (UBI-QEP) can provide in a straightforward manner information

on the methane activation barrier on Pd(1 1 1) at zero coverage. Calculations performed by assuming a direct dissociation of methane, as suggested by TAP experiments, lead to a higher value of the activation energy for the dissociative adsorption of methane than that calculated when oxygen ad-atoms assist the dissociation of methane, $CH_4 + OH_{ads} \rightarrow CH_{3ads} + H_2O$ instead of $CH_4 \rightarrow CH_{3,ads} + H_{ads}$ (67 vs. 38 kJ mol^{-1}). Such calculations can be tentatively compared with experimental activation barrier derived from TAP responses performed on pre-oxidized and pre-reduced Pd/Al_2O_3 and $Pd–Rh/Al_2O_3$ under UHV conditions. A qualitative agreement between theoretical values and experimental activation energy values measured on pre-oxidized and pre-reduced aged-Pd/Al_2O_3 samples shows that oxygen exhibits a beneficial effect in methane dissociation. Let us note that those theoretical data corresponding to very low surface coverage would not fit those obtained when raising the oxygen pre-coverage since Valden et al. [19] observed a lowering of the absolute dissociation probability in agreement with a first order kinetic with one oxygen atom capable to block two adjacent vacant adsorption sites. Some discrepancies also arise with activation energy calculated on freshly-prepared catalysts abnormally low with no significant impact of the thermal pre-treatment as above-mentioned. Such an observation emphasizes that an extra source of oxygen coming from the support would be involved in the activation of methane as earlier suggested [10,27,29,30]. In fact, alumina is well-recognized as a reservoir of OH groups and can participate to subsequent surface reactions taking place over noble metals sites via spill-over effects. As suggested above, the negative signal of water also reflects that water as side product may strongly (re)adsorb on alumina and spill-over from the support to noble metals further dissociating to produce H_2 and chemisorbed O atoms. The O atoms are prone to participate in a reaction with methane explaining the noticed decrease of water release when methane is pulsed into the reactor. The broad signal of hydrogen particularly at low temperature would suggest the occurrence of such processes. On the contrary, its strong attenuation on aged catalysts would suggest a strong alteration of the metal/support interface due to particle sintering especially on Pd-only catalyst. In this latter case, the influence of the thermal pre-treatment on the methane adsorption capacity would be restored while the preservation of the metal/support interface on $Pd–Rh/Al_2O_3$ would minimize the impact of the thermal treatment. Up to now most of those considerations have been essentially discussed qualitatively. Accurate calculations of activation energies provide quantitative evidences that correctly support previous observations.

4. Conclusion

Methane activation on Pd and Rh based catalysts has been investigated from TAP experiments. The outlet responses of methane have been modeled assuming a Knudsen diffusion regime with optimized values for the efficient diffusivity coefficients determined for all solid materials used in this study. In our operating conditions, irreversible adsorption of methane takes place with a large fraction of CH_4 converted to CO and H_2 on pre-reduced samples and CO_2 and H_2O on pre-oxidized catalysts. The most significant kinetic features were obtained on aged catalysts in wet atmosphere at 980 °C that induces significant thermal sintering of Pd particles partly inhibited when Rh is incorporated to Pd. Indeed, aged Pd/Al_2O_3 is sensitive to thermal pretreatments with a beneficial effect of oxygen while pre-coverage of oxygen has no significant effect on the adsorptive properties of aged $Pd–Rh/Al_2O_3$. Significant increase in the activation barrier on aged catalysts is observed which has been explained by an inhibition of the participation of oxygen-containing species to the methane adsorption on Pd/Rh particles due to aging. On aged catalyst, methane would be essentially activated over noble metal sites. Aged Pd/Al_2O_3, practically inactive in reduced form, would recover its activity after re-oxidation, due to the beneficial effect of oxygen characteristic of the adsorptive properties of Pd.

Acknowledgments

The authors would like to thank, the Staff of Comsol France for competent and friendly advice, the French agency of energy and environment (Ademe) and the North Region through the Institut de Recherche en Environnement Industriel (IRENI) for a fellowship (Y. Renème), Umicore company which supplied model NGV catalyst samples. Finally, we would like to thank Arnaud Beaurain and Martine Trentesaux who conducted XPS measurements.

Appendix A. Supplementary data

Supplementary data associated with this article can be found, in the online version, at http://dx.doi.org/10.1016/j.apcatb.2012.06.033.

References

[1] R. Burch, F.J. Urbano, P.K. Loader, Applied Catalysis A: General 123 (1995) 173–184.
[2] P. Gélin, M. Primet, Applied Catalysis B: Environmental 39 (2002) 1–37.
[3] B.C. Enger, R. Lodeng, A. Holmen, Applied Catalysis A: General 346 (2008) 1–27.
[4] J.R. Rostrup-Nielsen, J. Sehested, J.K. Norskov, in: B.C. Gates, H. Knozinger (Eds.), Advances in Catalysis, vol. 47, Elsevier Academic Press Inc, San Diego, 2002, pp. 65–139.
[5] D. Dissanayake, M.P. Rosynek, J.H. Lunsford, Journal of Physical Chemistry 97 (1993) 3644–3646.
[6] T.V. Choudhary, D.W. Goodman, Journal of Molecular Catalysis A: Chemical 163 (2000) 9–18.
[7] B. Xing, X.Y. Pang, G.C. Wang, Z.F. Shang, Journal of Molecular Catalysis A: Chemical 315 (2010) 187–196.
[8] C.T. Au, H.Y. Wang, Journal of Catalysis 167 (1997) 337–345.
[9] D.A.J.M. Ligthart, R.A. Van Santen, E.J.M. Hensen, Journal of Catalysis 280 (2011) 206–220.
[10] D. Wang, Z. Li, C. Luo, W. Weng, H. Wan, Chemical Engineering Science 58 (2003) 887–893.
[11] G.S. Yablonsky, M. Olea, G.B. Marin, Journal of Catalysis 216 (2003) 120–134.
[12] Y. Renème, F. Dhainaut, M. Trentesaux, B. Ravanbakhsh, P. Granger, C. Dujardin, L. Gengembre, P.L. De Cola, Surface Interface Analysis 42 (2010) 530–535.
[13] A.C. van Veen, O. Hinrichsen, M. Muhler, Journal of Catalysis 210 (2002) 53–66.
[14] A.C. van Veen, H.W. Zanthoff, O. Hinrichsen, M. Muhler, Journal of Vacuum Science and Technology 19 (2001) 651–655.
[15] P. Phanawadee, M. Phongaksorn, N. Chaimongkol, A. Jaree, J. Limtrakul, Chemical Engineering Journal 115 (2005) 51–62.
[16] J.T. Gleaves, G.S. Yablonskii, P. Phanawadee, Y. Schuurman, Applied Catalysis A: General 160 (1997) 55–88.
[17] J.P. Hong, S. Pietrzyk, A.Y. Khodakov, W. Chu, M. Olea, V. Balcaen, G.B. Marin, Applied Catalysis A: General 375 (2010) 116–123.
[18] M. Valden, J. Pere, N. Xiang, M. Pessa, Chemical Physics Letters 257 (1996) 289–296.
[19] M. Valden, J. Pere, M. Hirsimäki, S. Suhonen, M. Pessa, Surface Science 377–379 (1997) 605–609.
[20] I. Sack, V. Balcaen, M. Olea, H. Poelman, G.B. Marin, Catalysis Today 112 (2006) 68–72.
[21] V. Balcaen, I. Sack, M. Olea, G.B. Marin, Applied Catalysis A: General 371 (2009) 31–42.
[22] R. Vallabh, P. Banks-Lee, A.-F. Seyam, Journal of Engineered Fibers and Fabrics 5 (2010) 7–15.
[23] D.G. Huizenga, D.M. Smith, AIChE Journal 32 (1986) 1–6.
[24] I. Sack, A Kinetic Study of the Reduction and the Reoxidation of Vanadia-Based Catalysts by Temporal Analysis of Products, Department of Chemical Engineering and Technical Chemistry, Ghent University, Ghent, 2006, p. 254.
[25] C.N. Satterfield, Mass Transfer in Heterogeneous Catalysis, MIT Press, Cambridge, MA, 1970.
[26] O. Dewaele, G.F. Froment, Journal of Catalysis 184 (1999) 499–513.
[27] D. Wang, O. Dewaele, G.F. Froment, Journal of Molecular Catalysis A: Chemical 136 (1998) 301–309.
[28] E. Shustorovich, H. Sellers, Surface Science Reports 31 (1998) 1–119.
[29] Y. Schuurman, C. Marquez-Alvarez, V.C.H. Kroll, C. Mirodatos, Catalysis Today 46 (1998) 185–192.
[30] A.M. O'Connor, Y. Schuurman, J.R.H. Ross, C. Mirodatos, Catalysis Today 115 (2006) 191–198.